Available online at www.sciencedirect.com
ScienceDirect
Journal of Power Sources 165 (2007) 481–488
JOURNAL OF POWER SOURCES
www.elsevier.com/locate/jpowsour

# A microfabricated nickel–hydrogen battery using thick film printing techniques

Waiping G. Tam *, Jesse S. Wainright

*Department of Chemical Engineering, Case Western Reserve University, Cleveland, OH 44106, USA*

Received 30 September 2006; received in revised form 14 November 2006; accepted 17 November 2006
Available online 10 January 2007

**Abstract**

To utilize the distinctive cycle life and safety characteristics of the nickel–hydrogen chemistry while eliminating the high pressure limitations of conventional nickel–hydrogen cells, a microfabricated nickel–hydrogen battery using a low-pressure metal hydride for hydrogen storage is being developed for powering micro-electromechanical systems (MEMS) devices and for biomedical applications where the battery would be implanted within the body. Thick film printing techniques which are simple and low cost were used to fabricate this battery. Inks were developed for each of the different battery components, including the electrodes, current collectors and separator. SEM images on these printed components showed the desired characteristics for each. Positive electrode cycling tests were performed on the printed positive electrodes while cyclic voltammetry was used to characterize the printed negative electrodes. Consistent charge and discharge performance was observed during positive electrode cycling. Full cells with printed positive and negative assemblies were assembled and tested.


*Keywords:* Alkaline; Nickel–hydrogen batteries; Microfabrication; Thick film printing

## 1. Introduction

### 1.1. Nickel–hydrogen battery overview

The nickel–hydrogen (Ni–$H_2$) battery is a secondary alkaline battery combining battery and fuel cell technologies. Its positive electrode is a $Ni(OH)_2$/NiOOH electrode, commonly used in NiCd and NiMH batteries (Eq. (1)). The negative electrode is a hydrogen electrode on catalytic platinum, as commonly used in hydrogen–oxygen fuel cells (Eq. (2)). Concentrated potassium hydroxide ranging from 26 to 31 wt.% has been used as the battery electrolyte [1]. The net reaction of the battery during charge and discharge is shown in Eq. (3).

$$Ni(OH)_2 + OH^- \leftrightarrow NiOOH + H_2O + e^- \quad (1)$$

$$H_2O + e^- \leftrightarrow OH^- + \tfrac{1}{2}H_2 \quad (2)$$

$$Ni(OH)_2 \leftrightarrow NiOOH + \tfrac{1}{2}H_2 \quad (3)$$

where "→" shows charging reactions and "←" shows discharge reactions.

As the net reaction only involves hydrogen reduction of NiOOH to $Ni(OH)_2$ without a net change in the electrolyte concentration or in the amount of water within the battery, this battery chemistry is referred to as a maintenance-free battery. During overcharge, oxygen is evolved at the positive electrode, which will be recombined electrochemically at the catalytic negative electrode. Thus, the battery can tolerate continuous overcharge without any adverse effects. Moreover, the battery offers excellent cycle life, with over 40,000 cycles demonstrated at 40% depth of discharge (DOD) in low earth-orbit satellites [1].

#### 1.1.1. Limitations of conventional nickel–hydrogen batteries

A conventional Ni–$H_2$ battery relies on high-pressure hydrogen (55–70 atm) to provide the necessary hydrogen capacity to match the positive electrode capacity. The use of individual pressure vessels to seal the battery leads to high materials cost and complicated vessel sealing. In addition, many other mechanical components are needed for the battery assembly, taking up

* Corresponding author. Tel.: +1 216 262 6409.
*E-mail addresses:* waipingtam@yahoo.com (W.G. Tam), jesse.wainright@case.edu (J.S. Wainright).

0378-7753/$ – see front matter © 2006 Elsevier B.V. All rights reserved.
doi:10.1016/j.jpowsour.2006.11.042

additional volume and leading to low volumetric energy density. Additionally, for one of our intended uses, powering implantable biomedical devices, storing hydrogen at high pressure represented an unwelcome safety concern.

### 1.1.2. Motivation for microfabrication

As current successes in micro-electromechanical systems (MEMS) have been advancing, there is an urgent need for microscopic power sources [2]. Availability of these power sources will permit a truly integrated system to be fabricated, reducing fabrication complexity and increasing the range of potential applications.

In light of this demand, evaluating the possibility of microfabricating a Ni–$H_2$ battery using thick film printing is attractive. To eliminate the high-pressure hydrogen constraint of the conventional Ni–$H_2$ battery, the use of low-pressure metal hydride separated from the electrolyte is being developed for on-board hydrogen storage. As the metal hydride only acts as a hydrogen reservoir, metal hydride corrosion, which is the main mode of failure for the nickel–metal hydride battery, can be eliminated. Instead of using conventional fabrication techniques, we proposed the use of thick film printing to fabricate this battery. Thick film printing is inexpensive to set up and simple to use. Recently, this technique has been investigated for battery [3] and fuel cell [4] applications. The resulting battery should be small, light, and reliable, with exceptional cycle life.

### 1.1.3. Objective

The ultimate objective of this work is to use the thick film printing to fabricate a completely stand-alone sealed Ni–$H_2$ battery using low-pressure metal hydride for hydrogen storage. The resulting battery should be rechargeable, showing consistent charging and discharging performance upon cycling, and operate at near-ambient hydrogen pressure. The work shown below attempted to produce these goals, but the major focus was on investigating if thick film printing could be used to fabricate the positive and negative electrodes of a Ni–$H_2$ battery with rechargeable performance.

## 1.2. Design requirements and fabrication of microfabricated nickel–hydrogen battery components

Fig. 1 shows the basic Ni–$H_2$ battery design adopted for microfabrication. Ultimately, each battery component, except the porous substrate, will be thick film printed or sputter deposited. To ensure the battery performs properly, each battery component must be carefully designed and formulated. The discussion below will focus mainly on the positive and negative electrodes, and the positive and negative current collectors. Formulation and evaluation of the metal hydride material and the printable electrolyte/separator layer are presented elsewhere [5,6].

### 1.2.1. Battery substrate

For the battery configuration shown in Fig. 1, the battery substrate must be porous to allow for effective hydrogen diffusion into and out of the negative electrode. This also will

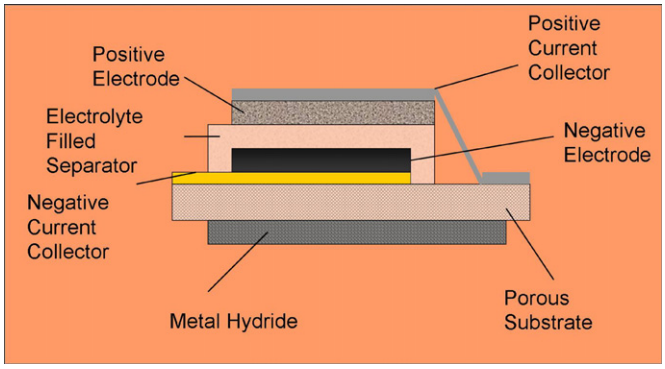


Fig. 1. Design of the Ni–$H_2$ battery for microfabrication.

allow oxygen evolved at the positive electrode during overcharging to recombine with the negative electrode, so as to maintain water balance within the battery. It should be noted that oxygen transport through the electrolyte is likely to be very slow compared to oxygen transport through the gas phase. As a result, oxygen produced during overcharge is assumed to react at the negative electrode after passing through the substrate. As each battery component is thick film printed layer by layer onto the substrate, it should also be mechanically robust to handle the pressure applied during printing and repeated baking during the fabrication process.

The substrate selected for this work was a Teflon membrane from GE Osmonics Labstore. The thickness was 50 μm thick with a pore size of 0.22 μm, and the membrane is stable up to 260 °C.

### 1.2.2. Positive current collector

Good electrical conductivity is the primary requirement for the positive current collector. Some porosity is required to allow oxygen produced on overcharge to escape into the gas phase. The positive current collector must also be stable within the cycling voltage range of the battery (∼1.1–1.5 V). For this purpose, ‘stable’ means that the current collector material will not corrode, and also that it is essentially unreactive with hydrogen and that oxygen evolution is negligible in the potential range of interest. Cyclic voltammetry tests with commercially available gold (Ercon R-464 (DPM-78)) and silver (Ercon E1400-136) based inks showed that both of these inks were unstable within the voltage range of the battery. Silver, while unreactive with hydrogen, continually oxidized, resulting in a loss of electrical conductivity. Gold remained conductive, and did not appreciably evolve oxygen within the potential range of interest. However, at the lower end of the potential range, gold is in the metallic state, and was observed to oxidize hydrogen. As a result, the effort was focused on developing a nickel-based ink for the positive current collector. The formulation of the nickel-based ink consisted of 50 vol.% filamentary nickel powder (Novamet, Inco Type 225, 2.2–2.8 μm) dispersed in a polyvinylidiene fluoride (PVDF) slurry with dimethyl formamide (DMF) as the solvent. The thickness of the printed collector after curing was 18 μm, as measured with a non-contact laser profilometer from Optical Gauging Products (OGP model ‘Cobra’). The electrical con-

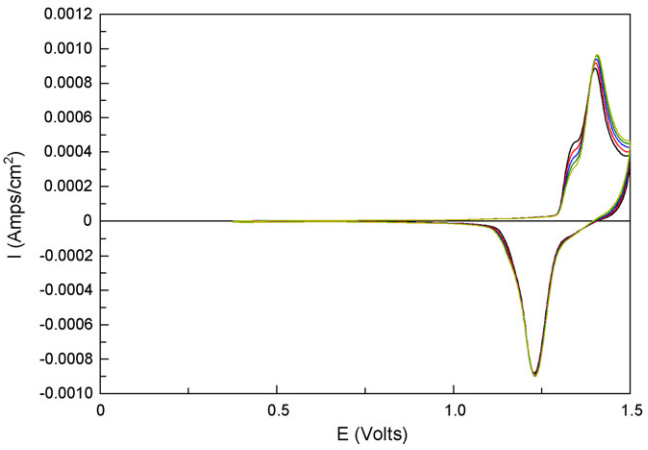


Fig. 2. Cyclic voltammetry results for the positive current collector ink.

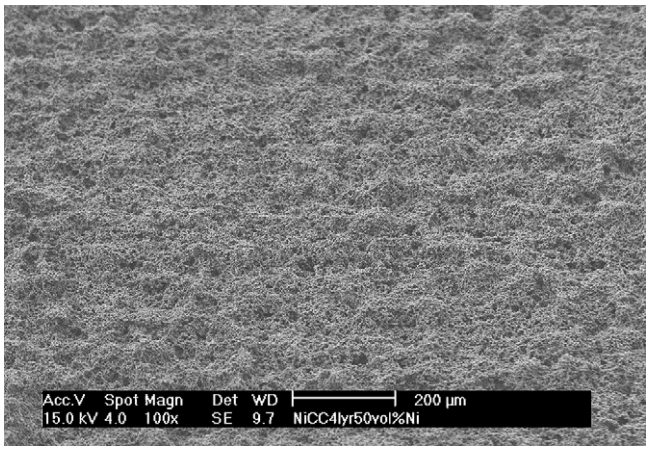


Fig. 3. SEM image of the surface of the positive current collector (100×).

ductivity of this ink when cured was measured to be 111 S $cm^{-1}$ using the four-point method.

Cyclic voltammetry was used to evaluate the stability of the in-house formulated nickel ink. The ink was first printed onto a porous Teflon substrate with a 1-$cm^2$ active area. A single piece of commercial platinum catalyzed gas diffusion electrode (Etek A-2 Silver-Plated Nickel Screen Electrode) of 1 $cm^2$ area was used as both the counter and reference electrode. Cyclic voltammetry tests performed using two of these commercial electrodes showed very little overpotential (less than 10 mV for currents up to 5 mA $cm^{-2}$), allowing this commercial electrode to serve as both the counter and reference electrode. An electrochemical cell was assembled by sandwiching the working and the counter/reference electrodes with a Celgard separator (3501) soaked with 26 wt.% KOH. The cell was clamped together to ensure close contact between the electrodes. The top and the bottom plates of the clamping assembly were perforated to allow gas flow around the cell during test. The cell assembly was then placed in a hydrogen purged chamber to maintain a constant hydrogen pressure. Cyclic voltammetry was performed at 1.4 psig hydrogen pressure from the open circuit voltage to +1.5 V versus the reference and back to the open circuit voltage at a 2 mV $s^{-1}$ scan rate.

In Fig. 2, the cyclic voltammetry results for the in-house formulated nickel current collector ink are shown. Nickel oxidation and reduction were observed at 1.40 and 1.23 V, respectively. An unknown anodic peak was also observed at 1.33 V whose height decreased upon cycling. This is thought to be due to impurities in the test sample that were oxidatively consumed. Oxygen evolution does take place as evidenced by the non-zero current at 1.5 V, after passing through the $Ni^{2+/3+}$ oxidation peak. At lower potentials, the relative extents of oxygen evolution and nickel oxidation cannot be quantitatively determined from the voltammetry, but oxygen evolution can be assumed to occur even at potentials as low as 1.4 V. Hydrogen oxidation on the nickel surface was not observed, as the nickel surface is always oxidized. However, after the first few scans, the peak currents associated with the nickel redox peaks do not increase, indicating that the surface of the nickel particles is essentially passivated, and that a conductive core remains.

In Fig. 3, an SEM image of the printed positive current collector surface at 100× is shown. Considerable roughness and porosity were observed on the current collector surface. Both characteristics were important for the positive assembly to function properly. The former allows the positive electrode to adhere well to the current collector while the latter allows efficient oxygen diffusion from the positive electrode during overcharge. The porosity was estimated to be 24%. In addition, the nickel powder appeared to be well mixed with the PVDF binder, providing a continuous path for the electrons to pass through. The in-house formulated nickel ink was therefore used as the positive current collector in the results described below.

### *1.2.3. Positive electrode*

For the positive electrode to function properly, efficient charge transfer must occur both from the current collector to the electrode and within the solid-state active material. Therefore, both electrical and ionic conductivity are critical for the electrode's performance and the ink formulation was varied to find an acceptable compromise of these properties.

β-Nickel hydroxide powder (Kansai Catalyst Co., Ltd.) was used as the positive active material. The 12-μm powder is 2.5 wt.% cobalt surface-coated and has a 4.5 wt.% zinc and 0.7 wt.% cobalt mixed in a solid solution within the nickel hydroxide. Polyacrylic acid potassium salt (PAAK) is used as a binder and 26 wt.% KOH solution was used as a solvent and to provide ionic conductivity within the electrode. Extra fine nickel powder (Novamet, Inco Type 210, 0.5–1 μm) was also added to further improve the electrical conductivity of the positive electrode. The fine nickel content was varied until the electrical conductivity exceeded 0.01 S $cm^{-1}$. This value was chosen to give an acceptable level of electrical conductivity without overly limiting the ionic conductivity or the electrode's amphour capacity. The resulting positive electrode ink has a composition of 15 vol.% fine nickel and 39 vol.% nickel hydroxide. The printed positive electrode with the current collector was around 200 μm thick as measured with the non-contact profilometer.

The electrical conductivity of the resulting ink was 0.065 S $cm^{-1}$ with a specific theoretical capacity of 100 mAh $g^{-1}$. An estimate of the ionic conductivity of this ink was made by

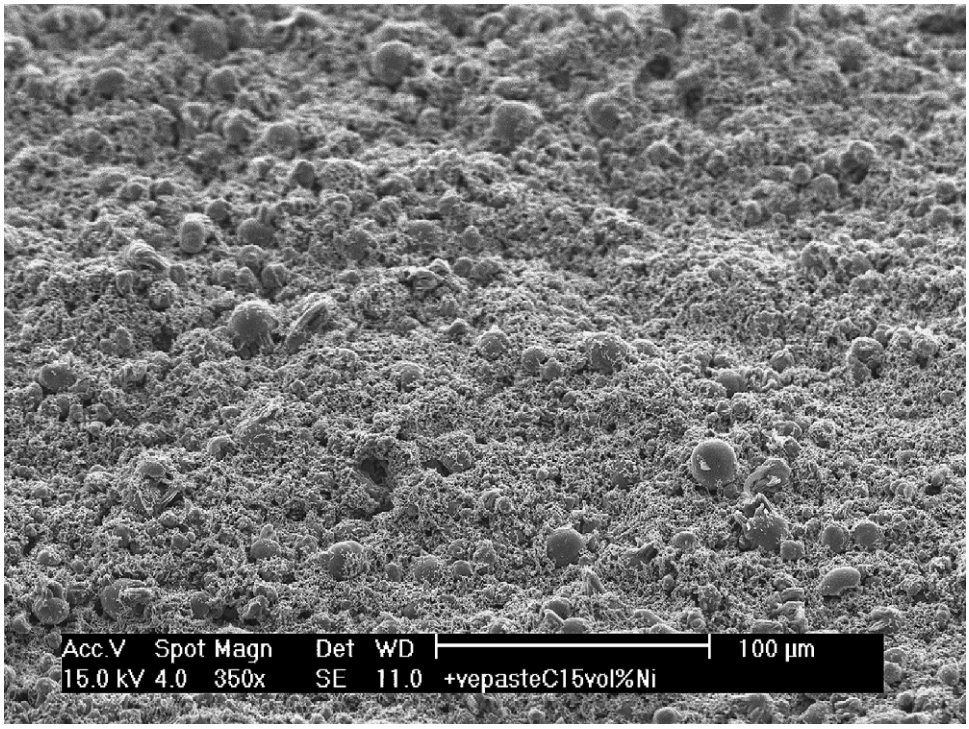


Fig. 4. SEM image of the surface of the positive electrode (350×).

comparing the impedance measured using a four-probe configuration at high and low frequencies. At high frequencies, both the electrical and ionic contributions to the conductivity are present in parallel. At low frequency, only the electrical conductivity of the ink is measured. The ionic conductivity within the positive electrode ink as measured in this manner was on the order of 1 mS $cm^{-1}$. Figs. 4 and 5 show the SEM images of the printed positive electrode's surface (350×) and cross-section (250×), respectively. A razor blade was used to cut across the positive assembly with caution to prevent disrupting the cross-section structure. Nickel hydroxide particles (spherical particles) were shown to be well distributed among the extra fine nickel metal powder (filamentary particles), and considerable porosity was observed throughout the surface and the cross-section.

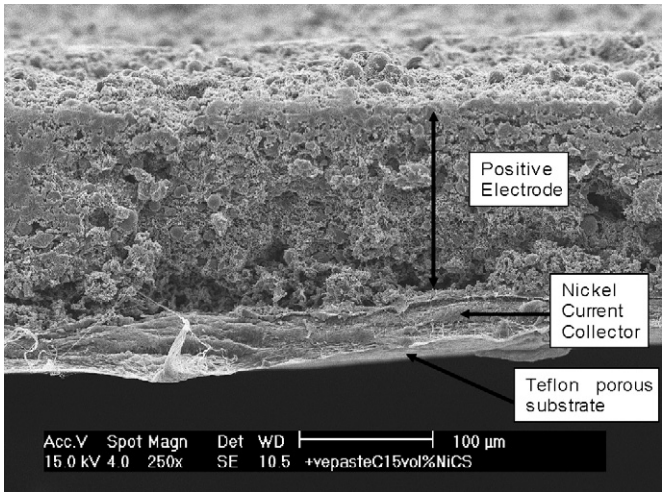


Fig. 5. SEM image of the cross-section of the positive electrode (250×).

As the extra fine nickel was added to enhance electrical conductivity of the positive electrode, good dispersion of the extra fine nickel was critical. Good porosity throughout the whole positive assembly allows efficient oxygen diffusion from the positive electrode during overcharge. The SEM images confirm that the printed positive electrode exhibits the desired characteristics for it to function properly.

### *1.2.4. Negative electrode*

Fast electrochemical kinetics for hydrogen oxidation and reduction are the main requirements for the negative electrode. The electrode should also be porous enough to allow efficient mass transfer of hydrogen into the electrode for hydrogen oxidation. Therefore, the thickness, porosity, and the platinum loading of the negative electrode were considered for the negative electrode performance. An ink based on platinum black (Alfa Aesar, #12755) in PVDF/DMF slurry was used in this work. This ink was printed to a platinum loading of 6.3 mg $cm^{-2}$. The average negative electrode thickness was about 77 μm, which is quite thick compared to those used in the microfabricated fuel cells [4]. This was achieved by using a thicker stencil in this work. The thicker electrode provided improved electrical conductivity necessary to provide good connectivity with the grid pattern of the negative current collector (see below). Four-point AC impedance measurements showed that the platinum black ink had an electrical conductivity of 31.8 S $cm^{-1}$.

Fig. 6 shows the SEM image of the negative electrode's surface at 350×. As with the positive electrode, considerable porosity is observed and the electrode material appears well mixed and homogeneous.

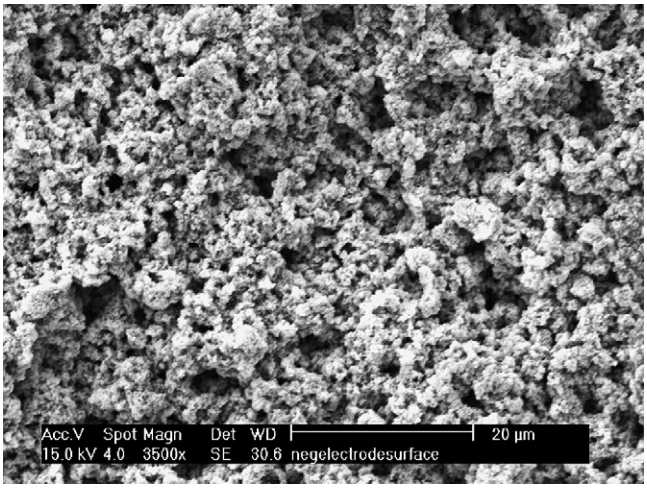


Fig. 6. SEM image of the negative electrode's surface (350×).

### 1.2.5. Negative current collector

Good electrical conductivity and compatibility with the negative electrode ink are the main requirements for the negative current collector. The current collector should also be porous to allow efficient transport of hydrogen into the negative electrode for hydrogen oxidation. Previous studies using a commercially available gold ink from Ercon Inc. (R-464 (DPM-78)) as the current collector in microfabricated fuel cells [4] showed sufficient porosity for adequate hydrogen transport. However, this ink is not compatible with the negative electrode ink as the solvent in the negative electrode ink (DMF) readily dissolves the binder in the Ercon gold ink. Thus, the Ercon gold ink could not be used as the negative current collector in this work.

To avoid incompatibility with the negative electrode ink, a thin gold pattern was sputter deposited as the negative current collector. To create the necessary porosity in the negative current collector, a grid pattern mask with 1.5 mm wide lines and 1 mm wide spaces between the lines was used to define the sputtered layer. A 5000-Å layer of metallic gold was sputtered onto the porous Teflon substrate to provide the necessary electrical conductivity. The gold sputtering was performed in the Center for Micro and Nano Processing at CWRU using a Denton Vacuum Discovery 18 Sputtering System.

## 2. Results and discussion

### 2.1. Positive electrode cycling with a commercial negative electrode

Positive electrode cycling tests were performed in the same manner as the voltammetry studies on the positive current collector with the positive electrode as the working electrode and the Etek platinum catalyzed gas diffusion electrode acting as both the counter and reference electrodes. The cell was assembled by sandwiching the working and the counter/reference electrodes with a Celgard separator (3501) soaked with 26 wt.% KOH. A constant hydrogen pressure was maintained at about 1.4 psig, in a chamber with a total volume of 100 $cm^3$. The hydrogen contained in the chamber is equivalent to 240 mAh, as compared to ≈1 mAh in the printed positive electrode. Thus, for these experiments, the hydrogen pressure is essentially constant and the battery is positive electrode limited. AC impedance spectroscopy was also used to monitor the cell solution resistance, taken as the real axis intercept at high frequency, after both charging and discharging for each cycle. Results from two essentially identical cells will be presented (cell details are shown in Table 1). The theoretical capacity of the positive electrode was determined by multiplying the specific theoretical capacity of the positive paste (100 mAh $g^{-1}$) by the amount of positive paste printed onto the positive current collector.

Table 1
Cell details for positive electrode cycling

| Cell ID | Positive electrode theoretical capacity (mAh) | Electrode thickness (μm) | Electrode area ($cm^2$) |
|---|---|---|---|
| 1 | 1.7 | 228 | 1.00 |
| 2 | 1.7 | 212 | 1.00 |

Formation of the positive electrode was performed at a *C*/24 rate based on 70% of the theoretical capacity. Typically after four or five cycles, a stable discharge capacity was obtained and the positive electrode was considered to be formed. The charge and discharge rates for further cycling were then changed to *C*/10 based on the actual capacity delivered after formation of the positive electrode. A 1.48 V cut-off voltage was applied during charging to avoid excessive oxygen evolution. The discharge cut-off voltage was 1.22 V.

The charge and discharge curves (*E* versus *Q*) for cell #2 during formation of the positive electrode are shown in Fig. 7. The arrows in the figure indicate the evolution of the curves with increasing number of cycles. A steady discharge capacity was observed after 5th cycle of 0.55 mAh $cm^{-2}$. Further cycling at the *C*/10 rate was performed as shown in Fig. 8. Consistent charging and discharging behavior was observed with the discharge capacity increasing slightly upon each cycle. The test was terminated after the 20th cycle due to time constraints; however, the results in Fig. 8 show that the electrode was still functioning

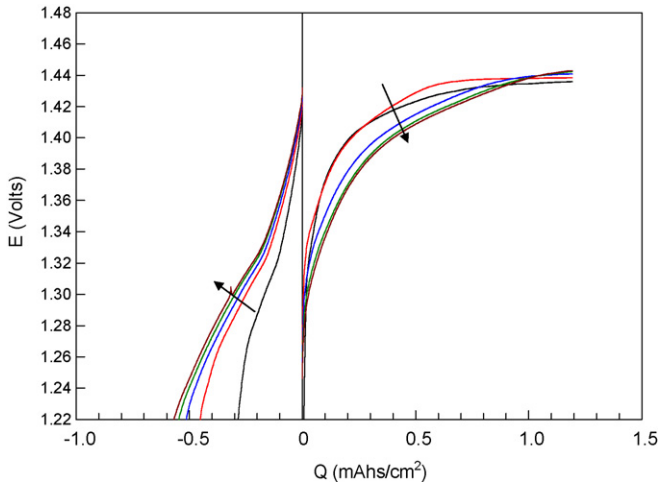


Fig. 7. Formation charging and discharging curves for cell #2.

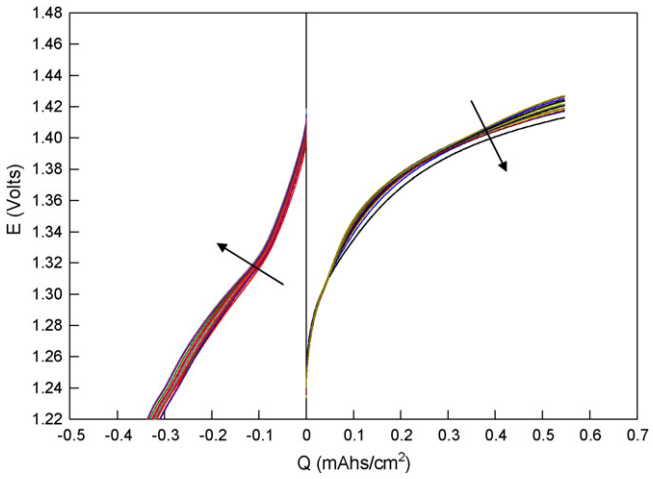


Fig. 8. Charging and discharging curves for the 5th to 20th cycles for cell #2.

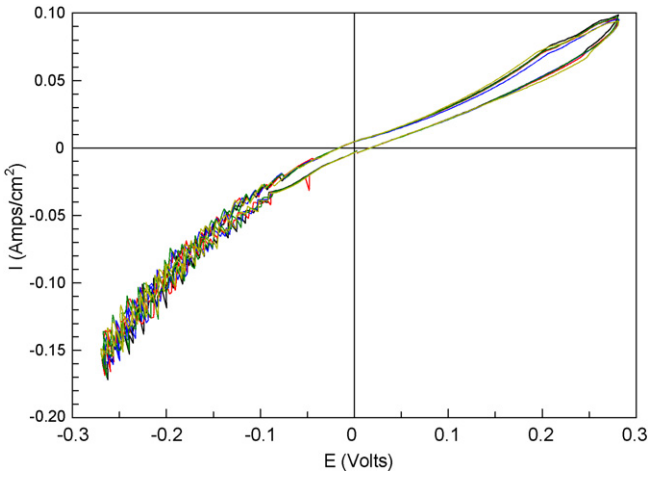


Fig. 9. CV results for the printed negative electrode based on platinum black.

in a stable manner and cycling could have been continued. The discharge capacity as of the 20th cycle was 0.34 mAh $cm^{-2}$. Similar results were also obtained for cell #1 for which the discharge capacity after the 20th cycle was 0.29 mAh $cm^{-2}$.

Although the discharge capacity increased with cycling, even after 20 cycles the cycle efficiency is poor with the voltage limits used. In Fig. 8, it can be seen that the intended 0.55 mAh $cm^{-2}$ is delivered to the positive electrode in each charge cycle as the charging voltage never reaches the 1.48 V cut-off. However, on discharge, the 1.22 V cut-off is reached relatively soon in each discharge cycle resulting in an amphour efficiency of <60%. This indicates that significant kinetic or mass transfer losses occur within the positive electrode on discharge and an improved formulation for this electrode is needed. The low amphour efficiency also indicates that there is considerable oxygen evolution occurring during charging, despite the fact that the potential never exceeds 1.43 V. The nickel hydroxide active material is treated with cobalt to improve its electrical conductivity, and also to increase the overpotential for oxygen evolution [7]. However, the positive electrode formulation also includes a substantial amount of the fine nickel powder, which is not cobalt treated, and oxygen evolution can occur on these surfaces at potentials below 1.5 V as shown in Fig. 2.

### 2.2. Negative electrode—cyclic voltammetry

Cyclic voltammetry tests were performed with the printed negative electrode as the working electrode and the commercial platinum catalyzed electrode as the counter/reference electrode. The electrochemical setup was the same as that used for the positive electrode cycling experiments with the hydrogen pressure maintained at 1.4 psig. For the negative electrode testing, the voltage was scanned from −0.3 to 0.3 V versus the quasi-reference at 2 mV $s^{-1}$. AC impedance spectroscopy was used to measure the cell solution resistance for IR correction.

The cyclic voltammetry results for the negative electrode fabricated with the platinum black ink are shown in Fig. 9. The IR free potential is plotted. A $H_2$ oxidation current density exceeding 100 mA $cm^{-2}$ was observed at the voltage extremes, without any obvious sign of mass transport limitation. At these current densities, the overpotential at the counter/reference electrode is not negligible; however, the conclusion that the negative electrode/negative current collector combination is sufficiently porous is still valid. The noise observed during the negative voltage regime is thought to be due to an unstable electrical connection. Based on the results shown in Fig. 9 and considering that the proposed battery will be operating at current densities from 10 μA $cm^{-2}$ to 1 mA $cm^{-2}$, the negative electrode overpotential will be well under 1 mV in operation, which is negligible. Thus, the platinum black ink on the sputtered current collector was shown to be an acceptable combination for this battery.

### 2.3. Full cell electrochemical testing

A full cell was assembled by sandwiching a positive assembly (Telfon membrane/printed positive current collector/printed positive electrode) and a negative assembly (Telfon membrane, sputtered current collector, printed negative electrode), around a Celgard separator (3501) soaked with 26 wt.% KOH. This cell was clamped together and placed in the hydrogen purge chamber, as described above. Formation and cycling procedures similar to those used in the positive electrode cycling test was used in the full cell testing, with cell details shown in Table 2.

Formation curves similar to those observed in the positive electrode tests were obtained in the full cell tests. The cell discharge capacity after the 5th cycle was 0.58 mAh. Further cycling was performed at *C*/12. Fig. 10 shows the cycling results after the formation cycles for the full cell.

Table 2
Cell details for full cell testing

| Positive electrode theoretical capacity (mAh) | Positive electrode thickness (μm) | Negative electrode thickness (μm) | Electrode area ($cm^2$) |
|---|---|---|---|
| 1.7 | 257 | 77 | 1.00 |

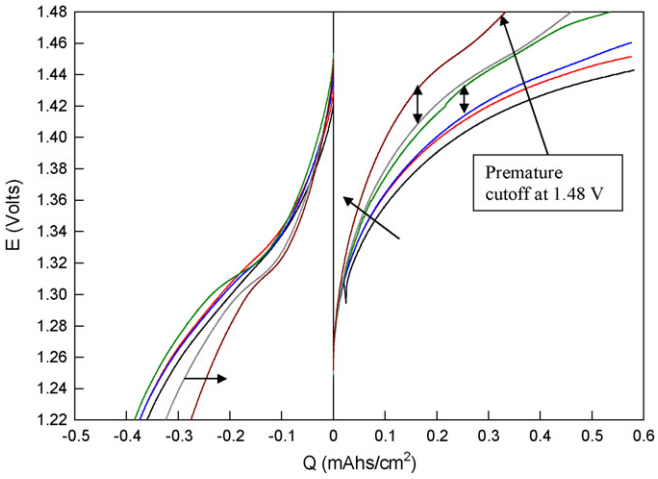


Fig. 10. Full cell cycling data from 6th to 12th cycles.

In Fig. 10, slightly increasing discharge capacity is seen from the 6th to 9th cycles; however, diminishing discharge capacity was observed after the 9th cycle due to premature charge cut-off at 1.48 V. In contrast to the results shown in Fig. 8, two sudden shifts in the charging curves were also observed as indicated by the double-headed arrows in Fig. 10.

The high frequency resistance at 20 kHz was measured after each half cycle and was observed to be increasing rapidly upon cycling, reaching ≈4.5 Ω-cm$^2$ after charge and 5.5 Ω-cm$^2$ after discharge at the end of 11th cycle. No sign of stabilization was observed. Regardless, based on this impedance data, the ohmic overpotential across the cell is at most ≈0.25 mV (0.0495 mA × 5 Ω = 0.25 mV). However, an overpotential increase of about 20 mV was observed in Fig. 10, suggesting that the cell was impeded by more than ohmic impedances. Fig. 11 shows the total cell impedance measured at 0.02 Hz. Similar to the high frequency results, the total cell impedance at 0.02 Hz was observed to be increasing rapidly, reaching ≈55 Ω-cm$^2$ at the end of 11th cycle; more than double the value measured after the 4th cycle. Since the impedance data at 0.02 Hz includes all impeding processes within the cell (ohmic, charge transfer, capacitive, mass transport), it shows that the cell became more and more resistive in general upon repeated cycling. The steepest increasing slope was observed

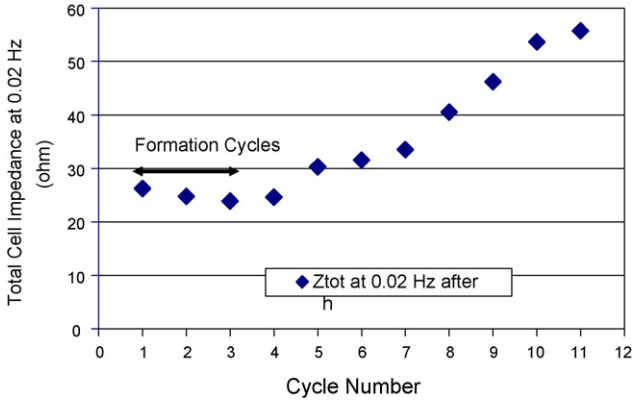


Fig. 11. Total cell impedance at 0.02 Hz upon cycling.

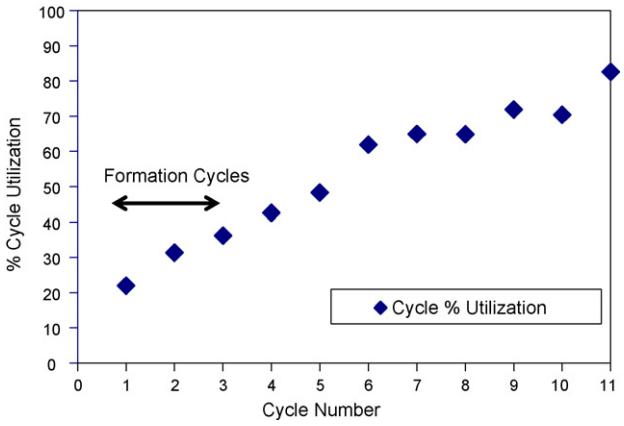


Fig. 12. %Cycle utilization upon cycling.

from the 7th to 10th cycles, in conjunction with the sudden shifts in the charging curves that were observed in Fig. 10. Clearly, the sudden shifts in charging curves are correlated with the rapidly increasing cell impedance.

The most likely explanation for the significant increase in the impedance of the cell is that the oxygen recombination and water balance within the cell are poor. During each charging cycle, oxygen is evolved. If it is not recombined with hydrogen at the negative electrode, the cell will tend to dry out. Furthermore, even if oxygen does recombine with hydrogen, it may not be readily redistributed throughout the cell [8]. Instead, water may accumulate within the negative assembly. In either case, the cell or portions of the cell will tend to dry out and it is likely that the result will be an increase in the cell impedance as was observed. In the results obtained with the commercial negative electrode (Fig. 8), there was substantial oxygen evolution, but this did not lead to the dramatic increase in the cell impedance that was seen with the printed negative assembly. From this, it can be surmised that oxygen evolution and subsequent water redistribution occur more effectively with the commercial negative electrode than with the printed negative assembly.

However, it should also be noted that the amphour efficiency (discharge capacity/charge capacity) was improving upon cycling as shown in Fig. 12. Utilization improved from 22% after the 1st cycle to 82.6% at the end of 11th cycle. The data suggested that although the deliverable capacity was diminishing due to premature cut-off as shown in Fig. 10, more of the charge capacity of the cell was able to be delivered upon cycling. This is a direct result of reaching the cut-off voltage, as charging is terminated before extended oxygen evolution can occur.

## 3. Conclusions

Inks for thick film printing were developed for several components of a microfabricated nickel–hydrogen battery, including the positive electrode, the positive current collector, and the negative electrode. Sputtered gold was used for the negative current collector to avoid solvent incompatibility with the negative electrode ink. SEM analysis performed on the printed positive electrodes, the printed positive current collector, and the printed

negative electrode showed the desired characteristics for each component to perform properly.

Electrochemical tests were performed separately for the printed positive electrodes and the printed negative electrodes against a commercial gas diffusion electrode. Consistent charge and discharge performance was observed during positive electrode cycling. A platinum black-based ink was shown to be an acceptable negative electrode ink with reasonable reactivity towards hydrogen oxidation and reduction and negligible mass transfer resistance. A full cell was assembled using the printed positive assembly and the printed negative assembly with a conventional electrolyte-soaked separator, and tested for cycling. Sudden upward shifts in charging curves and a corresponding rapid increase in the total cell impedance were observed during cycling. The increase in the cell impedance is thought to be related to poor oxygen recombination/water redistribution within the cell. However, an improvement in the cycle percent utilization was also observed, showing promise for acceptable cycling behavior if better control of the total cell impedance can be achieved.

## Acknowledgements

The authors would like to thank Dr. C.C. Liu and Ms. Laurie Dudik for their help with the thick film printing. The authors would also like to acknowledge NIH grants (NINDS R01-NS-41809) for financially supporting this work.

## References

[1] D. Linden, T.B. Reddy, Handbook of Batteries, McGraw-Hill, New York, 2001.
[2] P.B. Koeneman, I.J. Busch-Vishniac, K.L. Wood, J. Microelectromech. Sys. 6 (1997) 355.
[3] G.A. Ghiurcan, C.C. Liu, A. Webber, F.H. Feddrix, J. Electrochem. Soc. 150 (2003) A922.
[4] J.S. Wainright, R.F. Savinell, C.C. Liu, M. Litt, Electrochim. Acta 48 (2003) 2869.
[5] X. Shan, J.H. Payer, J.S. Wainright, J. Alloys Compd. 426 (2006) 400–407.
[6] J.S. Wainright, L. Dudik, manuscript in preparation.
[7] R.D. Armstrong, G.W.D. Briggs, E.A. Charles, J. Appl. Electrochem. 18 (1988) 215–219.
[8] B.K. Purushothaman, Ph.D. thesis, Case Western Reserve University, 2006.